Acta Crystallographica Section A
**Foundations of Crystallography**
ISSN 0108-7673

Received 15 March 2004
Accepted 19 July 2004



# The metal–insulator phase transition in mixed potassium–rubidium electro-sodalites

**Georg K. H. Madsen**

Department of Chemistry, University of Aarhus, DK-8000 Århus C, Denmark. Correspondence e-mail: georg@chem.au.dk

The collapse under pressure of the antiferromagnetic ground state of the potassium–rubidium electro-sodalite is studied using the linearized augmented plane wave with local orbitals method. Special considerations needed for setting up this basis for systems such as the electro-sodalites are discussed. It is demonstrated that the magnetism collapses at a unit-cell volume similar to potassium electro-sodalite and rubidium electro-sodalite. A critical pressure of 8 GPa is predicted. The mechanism behind the collapse is a mixing of the *F*-center states with the highly diffuse unoccupied *p* states of the alkali atoms.

## 1. Introduction

The use of porous framework compounds to encapsulate nanoscale atomic clusters gives several possibilities to produce novel materials. One example is the stabilization of magnetic nanoclusters inside the cavities of zeolites. The present study concerns the alkali electro-sodalites (AES). The AES are based on the sodalite framework which is the simplest of the zeolite structures and can be described as a body-centered cubic (b.c.c.) arrangement of $\beta$ cages. The sodalite studied here has two cages in each unit cell and consists of corner-sharing and regularly alternating $SiO_4$ and $AlO_4$ tetrahedra. Three alkali atoms ($A$) are needed inside each cage to balance the formal negative charge on the $AlO_4$ tetrahedra, leading to a unit-cell composition $A_6^{6+}(SiO_2)_6(AlO_2^-)_6$. There are four symmetry-equivalent alkali positions inside each cage, three of which are occupied in the basic sodalite, and the vacant site can be doped with one extra alkali atom. The extra alkali atom can be envisioned as contributing a cation to fill the vacant site and an electron. Thereby a paramagnetic $A_4^{4+}e^-$ cluster is formed inside each cage and, if every cage is doped, a b.c.c. array of paramagnetic clusters will be formed. This was first accomplished by Srdanov *et al.* (1992), who exposed a sodalite containing three Na ions per cage to sodium vapor. This resulted in a gradual color change from blue through purple to black eventually. The color change was ascribed to the formation of *F* centers.[1]

Two AES have been published, namely the sodium electro-sodalite [SES, $Na_8^{8+}e_2^{2-}(SiO_2)_6(AlO_2^-)_6$] and the potassium electro-sodalite [PES, $K_8^{8+}e_2^{2-}(SiO_2)_6(AlO_2^-)_6$]. When cooled below $T_N = 48 \pm 2$ K (SES) (Srdanov *et al.*, 1998) and $T_N = 71 \pm 2$ K (PES) (Damjanovic *et al.*, 2000), they undergo phase transitions and the b.c.c. sublattice of unpaired electrons order antiferromagnetically. At ambient pressure, the electronic structures of SES and PES are quite similar (Madsen, Iversen *et al.*, 2001): the bands belonging to the sodalite framework have a gap of approximately 5 eV and the *F* centers form a pair of narrow bonding–antibonding bands, approximately 1 eV broad, 1 eV below the sodalite conduction bands. The magnetism can be rationalized as the potential barrier of the negatively charged sodalite framework causing the *F*-center bands to narrow (Monnier *et al.*, 1994) and the *F*-center bands can be viewed as a half-filled band leading to the antiferromagnetic (AFM) ground state (Sankey *et al.*, 1998; Madsen, Iversen *et al.*, 2001).

The AES have shown a surprising behavior under pressure (Mizoguchi *et al.*, 2003; Madsen & Blaha, 2003). An experimental study of SES and PES under pressures up to 2.2 GPa reported two interesting findings. First of all, the ordering temperature ($T_N$) for both compounds decreases with increasing pressure (Mizoguchi *et al.*, 2003), which corresponds to a narrowing of the bands under pressure [using a simple one-band model of the magnetism (Sankey *et al.*, 1998; Madsen, Iversen *et al.*, 2001)]. Furthermore, the decrease in ordering temperature is much more pronounced in SES than in PES (Mizoguchi *et al.*, 2003). Although one would not expect a narrowing of bands with increasing pressure, both effects were also observed in a theoretical study (Madsen & Blaha, 2003). This study also found a substantial difference in critical pressure (CP) between SES (127 GPa) and PES (20 GPa). The theoretical study also included a hypothetical rubidium electro-sodalite [RbES, $Rb_8^{8+}e_2^{2-}(SiO_2)_6(AlO_2^-)_6$], which was found to have a CP of 13 GPa and to be electronically very similar to PES (Madsen & Blaha, 2003)

Recently, a mixed sodalite containing a $Rb_4^{4+}e^-$ cluster in every second cage and a $K_4^{4+}e^-$ cluster in every other [PRbES, $K_4^{4+}e^-Rb_4^{4+}e^-(SiO_2)_6(AlO_2^-)_6$] has been synthesized (Iversen & Srdanov, 2004). The inclusion of both K and Rb breaks the symmetry between neighboring cages. The AFM ordering of spins therefore no longer lowers the symmetry and it would be

[1] An *F* center (from German *Farbzentrum*) is an electron bound to a negative-ion vacancy. In this respect, the *F* centers in $Na_8^{8+}e_2^{2-}(SiO_2)_6(AlO_2^-)_6$ (SES) can be viewed as electrons occupying the positions of the chlorine vacancies of the well known $Na_8^{8+}Cl_2^{2-}(SiO_2)_6(AlO_2^-)_6$ sodalite in the $Na_4^{4+}e^-$ clusters.

interesting to see if the simple explanation of the AFM order (Sankey *et al.*, 1998; Madsen, Iversen *et al.*, 2001) still holds. Furthermore, it would be interesting to see if PRbES has a low CP like PES and RbES.

## 2. Computational approach

The computational approach employed in the present study is based on density functional theory (DFT) (see *e.g.* Baerends & Gritsenko, 1997, and references therein). The *WIEN2k* code (Blaha *et al.*, 2001), which expands the eigenfunctions of the Kohn–Sham equations using the linearized augmented plane wave (LAPW) (Andersen, 1975) method, is used.

### 2.1. APW-based methods

In APW schemes, the unit cell is divided into two regions: (i) the atomic sphere region, which consists of spheres centered at the atomic positions, inside which the basis functions, $\phi_{\mathbf{k}_n}$, satisfy the atomic Schrödinger equation; and (ii) the interstitial region, $I$, where the $\phi_{\mathbf{k}_n}$ consist of PWs. A basis function can thus be written as

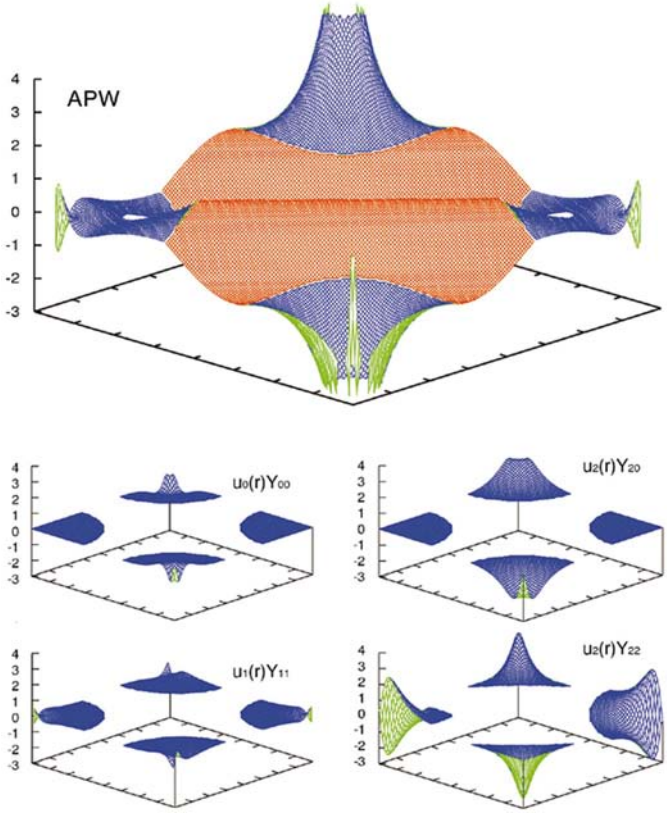


**Figure 1**
Example of the real part of an APW basis function. The APW is plotted in the (001) plane of b.c.c. Fe and corresponds to $\mathbf{K} = (1, 1, 0)2\pi/a$ and $\mathbf{k} = (1/4, 1/4, 0)2\pi/a$. The blue regions correspond to the atomic spheres and the red to the interstitial. The small plots below show different components of the basis function inside the sphere. The components not shown are either zero in this plane or simple mirror images of the ones shown.

$$\phi_{\mathbf{k}_n}(\mathbf{r}) = \begin{cases} \sum_{t,lm} a_{lm}^{t\mathbf{k}_n} u_l^t(r'; \varepsilon) Y_{lm}(\hat{\mathbf{r}}') & r' < R^t \\ \Omega^{-1/2} \exp(i\mathbf{k}_n \cdot \mathbf{r}) & \mathbf{r} \in I, \end{cases} \quad (1)$$

where $t$ refers to a given atomic sphere and $\mathbf{r}' = \mathbf{r} - \mathbf{r}_t$, where $\mathbf{r}_t$ is the atomic position within the unit cell. $\Omega$ is the unit-cell volume, $R^t$ the radius of the atomic sphere, $\mathbf{k}$ is a wavevector in the irreducible Brillouin zone, $\mathbf{K}$ a reciprocal-lattice vector and $\mathbf{k}_n = \mathbf{k} + \mathbf{K}$. $u_l^t$ is the numerical solution to the radial Schrödinger equation at the energy $\varepsilon$. The coefficients $a_{lm}^{t\mathbf{k}_n}$ are chosen such that the atomic functions match the corresponding PW at the sphere boundary. An example of an APW basis function is shown in Fig. 1.

The main problem of an APW basis set is that inside the spheres a Kohn–Sham orbital $\psi_{\mathbf{k},i}$ can only be accurately described if $\varepsilon$ is equal to the eigenenergy of $\psi_{\mathbf{k},i}$. This problem was solved by augmenting the basis set with radial functions that are the energy derivative of $u_l$, $\dot{u}_l$, leading to the LAPW method (Andersen, 1975). The Taylor expansion of $u_l(r; \varepsilon)$ around a given energy $\varepsilon_l$,

$$u_l(r; \varepsilon) = u_{1l}(r; \varepsilon_l) + (\varepsilon - \varepsilon_l)\dot{u}_l(r; \varepsilon_l) + O[(\varepsilon - \varepsilon_1)^2]$$

shows that the basis set thereby obtains a flexibility sufficient to describe radial functions in an energy range around a chosen linearization energy, $\varepsilon_l$. The LAPW method has been further improved by introducing local orbitals (LOs) to augment the LAPW basis set for certain $l$ values (Singh, 1991) and in its newest, and computationally most efficient, version the linearizing terms are also included in LOs (Sjöstedt *et al.*, 2000; Madsen, Blaha *et al.*, 2001). As will be discussed later, the $\varepsilon_l^t$ values can be chosen automatically during the self-consistent procedure. A useful quantity for the chemical interpretation of the calculated wavefunction is the partial $l$-like charge. In the APW method, these partial charges are often called $q_l^t$ (Blaha & Schwarz, 1983), where $t$ refers to a given atomic sphere. They can be defined as

$$q_l^t = (1/N) \sum_m \sum_{\mathbf{k},i} \langle \psi_{\mathbf{k},i} | Y_{lm}^t \rangle \langle Y_{lm}^t | \psi_{\mathbf{k},i} \rangle. \quad (2)$$

Similarly to the density of states (DOS), one can define an energy-projected $q_l^t$ as

$$q_l^t(\varepsilon) = (1/N) \sum_m \sum_{\mathbf{k},i} \langle \psi_{\mathbf{k},i} | Y_{lm}^t \rangle \langle Y_{lm}^t | \psi_{\mathbf{k},i} \rangle \delta(\varepsilon - \varepsilon_{\mathbf{k},i})/\mathrm{d}\varepsilon. \quad (3)$$

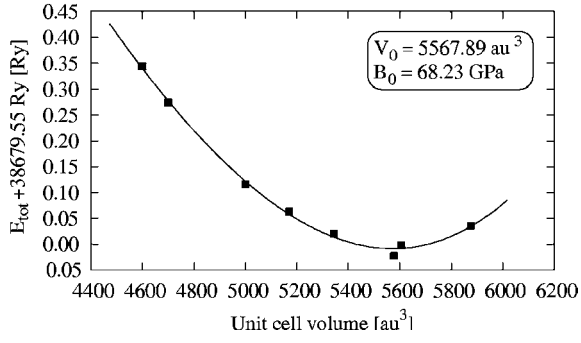


**Figure 2**
Total energy per unit cell of PRbES as a function of unit-cell volume.

The results of an LAPW calculation are relatively insensitive to the choice of linearization energies but $\varepsilon_l^t$ should be chosen to lie in the energy range where the states have a large contribution of $l$-like character from atom $t$. A non-standard option implemented in the *WIEN2k* code sets the linearization energies in each self-consistent loop at the weighted means of $q_l^t(\varepsilon)$, $\varepsilon_l = [\sum \varepsilon q_l^t(\varepsilon)]/q_l^t$. The advantage of this procedure for setting the linearization energies, especially when working on systems with unusual electronic structures such as the AES, will be discussed in the following sections.

### 2.2. Computational details

For the present study, sphere radii of 2.0, 2.0, 1.7, 1.55 and 1.5 a.u. were used for K, Rb, Al, Si and O, respectively. Calculations were performed at a plane-wave cut-off defined by $\min(R^t)\max(k_n) = 5.5$ corresponding to approximately 3850 APWs in the smallest unit cell and 4900 APWs in the largest. The exchange and correlation potentials of DFT were calculated using the generalized gradient approximation (Perdew *et al.*, 1996).

When the symmetry between the two cages in the unit cell is broken, the space-group symmetry is lowered from the $P\bar{4}3n$ space group (of SES and PES) to the $P23$ subgroup (of PRbES), which doubles the number of free positional parameters. No experimental information is available on the structure of PRbES, but the earlier calculated structures for SES and PES gave bond distances deviating only 1% from the experimental (Madsen & Blaha, 2003). We have therefore also optimized the structure of PRbES by varying the unit-cell volume and at each volume optimizing the free positional parameters using the analytical force expression for the LAPW basis set (Yu *et al.*, 1991; Madsen, Blaha *et al.*, 2001).

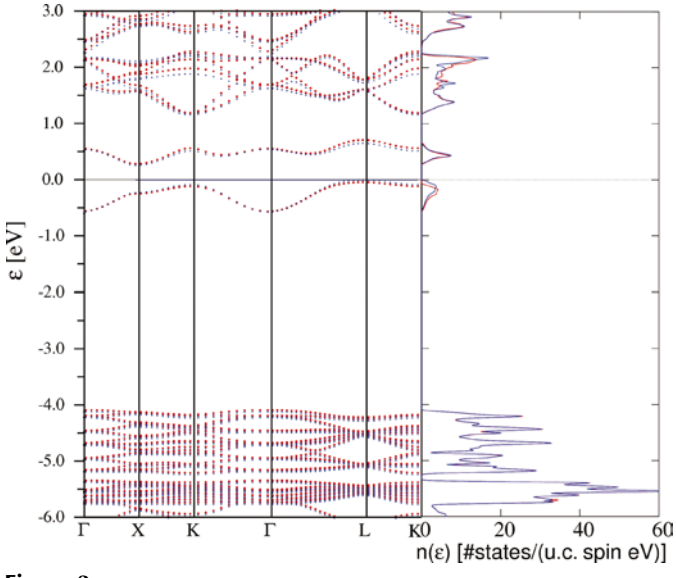


**Figure 3**
Band structure and DOS in NM-PRbES. The symbols label special points within the first Brillouin zone. Γ: $\mathbf{k} = (0, 0, 0)$, $X$: $\mathbf{k} = (1, 0, 0)\pi/a$, $K$: $\mathbf{k} = (1, 1, 0)\pi/a$, $L$: $\mathbf{k} = (1, 1, 1)\pi/a$. Red indicates the spin-up bands situated mainly in the cages containing Rb atoms. Blue indicates the spin-down bands situated mainly in the cages containing K atoms.

**Table 1**
Calculated cell axes and bond distances at ambient pressure for PRbES .

For comparison, the experimental (Madsen *et al.*, 1999; Madsen, Iversen *et al.*, 2001) and calculated (Madsen & Blaha, 2003) bond distances are also given for SES, PES, RbES. The unit for all entries is Å. The optimized fractional coordinates (atom, $x$, $y$, $z$) in the $P23$ space group are: (Si, 0.2498, 0, 1/4), (Al, 0.2497, 0.5, 0), (O1, 0.1447, 0.4796, 0.1540), (O2, 0.9816, 0.3553, 0.3461), (K, 0.1837, 0.1837, 0.1837), (Rb, 0.6752, 0.3248, 0.3248).

| | PRbES | SES | | PES | | RbES |
|---|---|---|---|---|---|---|
| | (calc.) | (exp.) | (calc.) | (exp.) | (calc.) | (calc.) |
| $a$ | 9.38 | 8.86 | 8.88 | 9.25 | 9.33 | 9.43 |
| Si—O | 1.64 | 1.62 | 1.65 | 1.64 | 1.64 | 1.64 |
| Al—O | 1.76 | 1.76 | 1.76 | 1.74 | 1.76 | 1.76 |
| O—Na | | 2.33 | 2.32 | | | |
| O—K | 2.81 | | | 2.72 | 2.74 | |
| O—Rb | 2.96 | | | | | 2.91 |

The energy *versus* volume curve is shown in Fig. 2. The equilibrium volume ($V_0$) and bulk moduli ($B_0$ and $B_0'$), Fig. 2, were calculated by fitting an equation of state (EOS) (Alchagirov *et al.*, 2001) to the calculated energies.

## 3. Results and discussion

### 3.1. Geometry and volume optimization

Table 1 shows that the calculated unit-cell volume of PRbES lies between that of PES and RbES. It is worth noting that, although Si and Al have one free positional parameter in the $P23$ space group, they hardly move from the high-symmetry positions of the $P\bar{4}3n$ space group. The lower symmetry also means that there are two non-equivalent

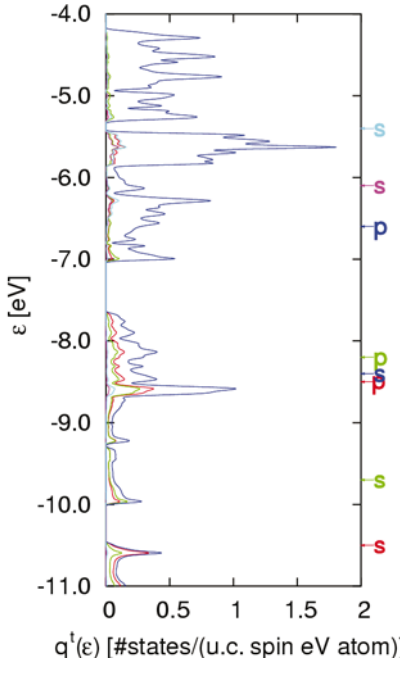


**Figure 4**
Atom projected DOS, $q^t(\varepsilon)$. The red line corresponds to Si, green to Al, blue to O, purple to K and cyan to Rb atoms. The linearization energies are marked to the right in corresponding colors.

O-atom positions. The four Si—O distances are therefore no longer forced to be equal, but in fact turn out to differ by only approximately 0.001 Å. In the $P\bar{4}3n$ space group, the faces of the Si—O and Al—O tetrahedra have two short edges and one long. In the $P23$ space group, all three edge lengths can be different, which does lead to a small distortion of approximately 0.01 Å of the short edges.

### 3.2. Ambient pressure electronic structure

Like the earlier studied AES, an AFM ordering of spins in PRbES is found to be the most stable energetically at ambient pressure, (Fig. 5*a*). The band structure and DOS of AFM-PRbES are shown in Fig. 3. The band structure is similar to the ones found for the other AES, with a 5 eV gap between the bonding and antibonding framework states and two *F*-center bands, approximately 1 eV broad, at the Fermi level. As the two cages in the unit cell are not symmetry equivalent, the two spins are no longer exactly the same. However, Fig. 3 shows that despite the broken symmetry the two bands are still very similar, in accordance with the earlier observation that PES and PRbES are electronically very similar (Madsen & Blaha, 2003).

Fig. 3 illustrates the need for special care when setting the linearization energies for the AES. Usually, setting the linearization energies of the *s* and *p* states 1.5–2.5 eV below the Fermi energy will place them in the desired energy interval. However, in the AES such a procedure would mean that the linearization energies would be set in an energy range where there are no states (Fig. 3). Instead, the linearization energies can be set at the weighted mean of $q_l^t(\varepsilon)$, as described in the previous section. The $q^t(\varepsilon)$ for the valence framework bands and the resulting linearization energies are shown in Fig. 4. Not surprisingly, the valence bands belong mainly to the O atoms but with some covalent contribution from the Si and Al atoms. The alkali atoms are mainly ionically bound and hardly contribute to these bands. The *F*-center bands are not shown in Fig. 4 because they are primarily situated in the interstitial spaces and therefore only have a very small contribution from the atomic spheres.

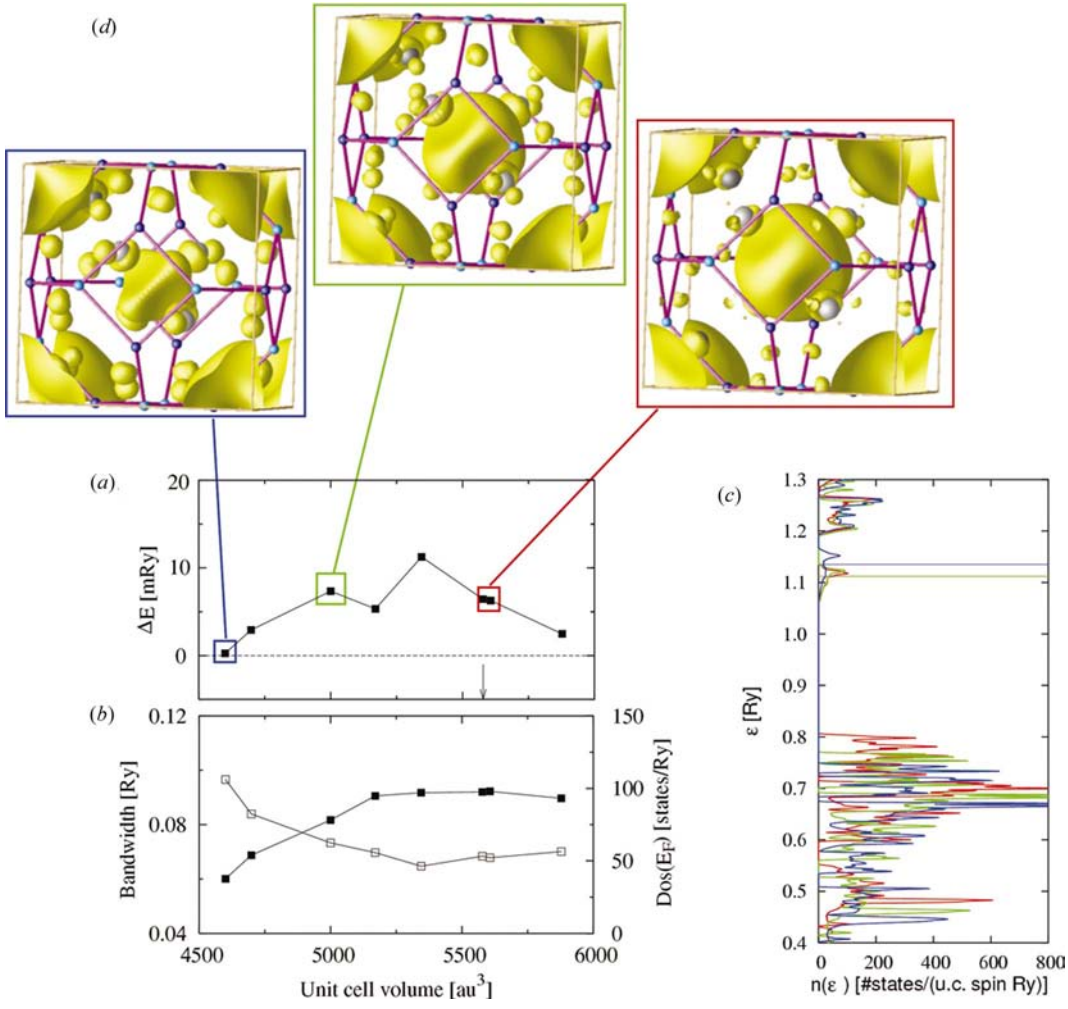


**Figure 5**
(*a*) Total energy difference between the nonmagnetic and antiferromagnetic states of PRbES. The optimized unit-cell volume is marked with an arrow. (*b*) Band width of *F*-center state (open points) and DOS ($E_F$) (filled points) for the NM state. (*c*) DOS at three volumes. The zero point is set at the energy of the potassium 3*p* state. The colors correspond to the marked points in (*a*). (*d*) Isosurface plots of the electron density from the occupied *F*-center states at three different volumes. The isosurface is set at 0.006 e Å$^{-3}$.

### 3.3. Pressure-induced phase transition

Fig. 5(*a*) shows the difference in energy between the non-magnetic (NM) and the AFM state. When the unit-cell volume is compressed to around 4600 a.u.$^3$, the magnetism collapses and the NM and AFM states become equal in energy. Using the calculated EOS, Fig. 2, a unit-cell volume of 4600 a.u.$^3$ corresponds to a pressure of 8.2 GPa. In addition, Fig. 5(*b*) shows that the *F*-center bands initially narrow slightly under pressure in accordance with both the experimental and theoretical results for PES and RbES (Madsen & Blaha, 2003). When the unit cell is further compressed, the bands broaden again, which eventually leads to the collapse of magnetism.

The mechanism behind the collapse of magnetism was discussed in an earlier paper (Madsen & Blaha, 2003). The collapse was found to coincide with the hybridization of the *F*-center bands with the unoccupied *p* states of the alkali atoms. This observation was used to explain the low CP for PES and RbES. While the 3*p* states of sodium are high in energy compared to the occupied states (situated 2.5 Ry above the 2*p* semi-core states), the 4*p*/5*p* states in atomic potassium/rubidium are much lower, lying 1.4 Ry/1.2 Ry above the 3*p*/4*p* semi-core states. In accordance, the Fermi level, when the magnetism collapses, is found 2.3 Ry/1.3 Ry/1.1 Ry above the Na 2*p*/K 3*p*/Rb 4*p* semi-core states in SES/PES/RbES, respectively. Fig. 5(*c*) shows that a similar mechanism can be used for PRbES. As the magnetism collapses and the *F*-center states broaden due to hybridization, the Fermi energy rises 1 Ry above the Rb 4*p* states and 1.1 Ry above the K 3*p* states.

The mixing of the *F*-center states with the diffuse *p* states also changes the charge density from the states at the Fermi level, Fig. 5(*d*). At ambient pressure, this density is close to spherical and situated at the center of the alkali tetrahedra. As pressure is applied, the electrons are redistributed towards the faces of the alkali tetrahedra and the *F* center is split into four maxima approximately midway between the Na atoms in two neighboring cages, Fig. 5(*d*).

## 4. Conclusions

It has been predicted that the magnetism in PRbES will collapse at a similar volume to PES and RbES and that a similar mechanism seems to apply. Furthermore, it has been shown that the LAPW basis as implemented in *WIEN2k* (Blaha *et al.*, 2001) forms a suitable basis for such compounds. As the basis-set quality is essentially controlled by only one parameter, the plane-wave cut-off, it is a simple task to systematically improve the basis set until convergence is reached. This implies that one does not need to have preconceived ideas about the 'chemistry' of the system to construct an efficient basis. The advantage is clearly seen by a comparison with our original study of the electron density in SES (Madsen *et al.*, 1999). To get the *F*-center state, the original atom-centered Gaussian basis set had to be augmented either by diffuse *p* functions on the Na atoms or by a floating Gaussian at the center of the cage. This procedure was justified by the large drop in total energy, but would not have been possible without specifically looking for the *F*-center state.

## References


Alchagirov, A. B., Perdew, J. P., Boettger, J. C., Albers, R. C. & Fiolhais, C. (2001). *Phys. Rev. B*, **63**, 224115.

Andersen, O. K. (1975). *Phys. Rev. B*, **12**, 3060–3083.

Baerends, E. J. & Gritsenko, O. V. (1997). *J. Phys. Chem. A*, **101**, 5383–5403.

Blaha, P. & Schwarz, K. (1983). *Int. J. Quantum Chem.* **23**, 1535–1552.

Blaha, P., Schwarz, K., Madsen, G. K. H., Kvasnicka, D. & Luitz, J. (2001). *WIEN2k, An Augmented Plane Wave Plus Local Orbitals Program for Calculating Crystal Properties*. ISBN 3-9501031-1-2. Vienna University of Technology, Austria.

Damjanovic, L., Stucky, G. D. & Srdanov, V. I. (2000). *J. Serb. Chem. Soc.* **65**, 311–314.

Iversen, B. B. & Srdanov, V. I. (2004). Personal communication.

Madsen, G. K. H. & Blaha, P. (2003). *Phys. Rev. B*, **67**, 85107.

Madsen, G. K. H., Blaha, P., Schwarz, K., Sjöstedt, E. & Nordström, L. (2001). *Phys. Rev. B*, **64**, 195134.

Madsen, G. K. H., Gatti, C., Iversen, B. B., Damjanovic, L., Stucky, G. D. & Srdanov, V. I. (1999). *Phys. Rev. B*, **59**, 12359–12369.

Madsen, G. K. H., Iversen, B. B., Blaha, P. & Schwarz, K. (2001). *Phys. Rev. B*, **64**, 195102.

Mizoguchi, K., Yamabe, T., Sakamoto, H., Damjanovic, L. & Srdanov, V. I. (2003). *Synth. Met.* **137**, 909–910.

Monnier, A., Srdanov, V. I., Stucky, G. D. & Metiu, H. (1994). *J. Chem. Phys.* **100**, 6944–6952.

Perdew, J. P., Burke, K. & Ernzerhof, M. (1996). *Phys. Rev. Lett.* **77**, 3865–3868.

Sankey, O. F., Demkov, A. A. & Lenosky, T. (1998). *Phys. Rev. B*, **57**, 15129–15139.

Singh, D. (1991). *Phys. Rev. B*, **43**, 6388–6392.

Sjöstedt, E., Nordström, L. & Singh, D. J. (2000). *Solid State Commun.* **114**, 15–20.

Srdanov, V. I., Haug, K., Metiu, H. & Stucky, G. D. (1992). *J. Phys. Chem.* **96**, 9039–9043.

Srdanov, V. I., Stucky, G. D., Lippmaa, E. & Engelhardt, G. (1998). *Phys. Rev. Lett.* **80**, 2449–2452.

Yu, R., Singh, D. & Krakauer, H. (1991). *Phys. Rev. B*, **43**, 6411–6421.